Turkish Journal of Electrical Engineering & Computer Sciences

http://journals.tubitak.gov.tr/elektrik/

Research Article

Turk J Elec Eng & Comp Sci
(2019) 27: 46 – 57

doi:10.3906/elk-1806-35

Improving side lobe level of X-band microstrip Rotman lens utilizing nonuniform distribution of output ports

Ehsan ZAREIAN-JAHROMI[1,*], **Raheleh BASIRI**[1], **Parvin SALEHI**[1], **Hamidreza KARAMI**[2]
[1]Department of Electrical and Electronics Engineering, Shiraz University of Technology, Shiraz, Iran
[2]Department of Electrical Engineering, Bu-Ali Sina University, Hamedan, Iran

Received: 04.06.2018 • **Accepted/Published Online:** 06.11.2018 • **Final Version:** 22.01.2019

Abstract: A new microstrip Rotman lens with enhanced side lobe level (SLL) is proposed for X-band applications. A proper nonuniform distribution of the initial width of output ports is considered to improve the SLL. The benefit of SLL improvement is not based on using additional attenuators or amplifiers at the output ports. Moreover, an analytical background is presented to investigate the resulting SLL of the proposed structure. The advantage of SLL enhancement is obtained at all noncorner scan angles considering 10 GHz operating frequency. As the middle input port is excited, more than 3 dB of SLL enhancement is achieved at 10 GHz. The proposed structure provides even more accurate scan angles than those of the conventional Rotman lens. The designed structure is simulated using full-wave HFSS 15 software. The comparison between simulated results and measurements of the fabricated proposed Rotman lens shows good agreement.

Key words: Antenna arrays, beam forming network, beam steering, side lobe level improvement, Rotman lens

1. Introduction

Beam steering antennas are encountered in numerous applications such as biomedical imaging, automotive anticollision radars, and communications [1–3]. Providing proper amplitude and phase distributions is essential in these radiating components. A beam-forming network (BFN) is a device producing desirable amplitude and phase distributions at its output ports. BFNs can be categorized into different structures including digital BFNs, network BFNs, and lens BFNs [4]. In 1950, Ruze designed a lens consisting of two perfect off-axis symmetrical focal points and an on-axis focal point [5]. In 1957, a bootlace lens was proposed by Gent [6]. Rotman et al. introduced a new lens structure consisting of three perfect focal points [7]. A symmetrical lens was introduced by Shelton as a modification to the Rotman lens structure [8]. In 1984, an improved Rotman lens design resulting in reduced phase-error was presented by Katagi et al. [9]. In 1991, Hansen reformulated the design procedure of the Rotman lens [10]. In this work, the effect of design parameters on the phase and amplitude errors has been investigated. Rao proposed three-dimensional lens BFNs considering four perfect focal points [11, 12].

The Rotman lens is a passive lens BFN that is in demand due to its many features including low cost, simplicity, reliability, and wide scanning angle [13]. The Rotman lens is a true-time-delay BFN and hence is capable of providing wideband beam steering. Rotman lens structures have been implemented in different configurations using waveguides, microstrips, striplines, and surface wave supporting waveguides [14, 15].

*Correspondence: zareian@sutech.ac.ir

Although the optimum side lobe level (SLL) of a uniform array is about 13 dB [16], it is difficult to obtain this threshold in practice due to unwanted multiple reflections resulting from the side walls, dummy ports, and array ports [17]. A modified Butler feeding network with 180° power dividers was proposed in [18], resulting in low SLL. A synthesized radiation pattern with low side lobes was introduced using a Rotman lens structure fed by a power divider in [14]. The beam ports are simultaneously excited with appropriate amplitudes to form the desired radiation pattern. Therefore, the proposed setup does not support beam steering in different directions. In [19], a proper weighting function was applied to the output ports, improving the SLL. This procedure demands additional attenuators or amplifiers at the output ports, which leads to reduced antenna efficiency or additional complexity, respectively.

In this paper, a new microstrip Rotman lens with enhanced SLL is presented, which is not based on using additional attenuators or amplifiers at the output ports. First, the positions of the input and output ports are optimized using a genetic algorithm (GA). Then the initial width of output ports is altered in order to manipulate the amplitude distribution at the output ports and hence improve the resulting SLL. The proposed structure includes seven input ports and eight output ports, and it provides a 45° scanning angle with 7.5° steps. As the middle input port is excited, more than 3 dB of SLL enhancement is achieved at the central operating frequency. The benefit of SLL improvement is obtained for all steering directions except side values, $\pm 22.5°$, at 10 GHz. The effect of altering the initial width of output ports on the resulting scan angles is also investigated. It is found that the proposed Rotman lens yields more accurate steering directions than the conventional Rotman lens at the central operating frequency.

This manuscript is organized as follows. In Section 2, the conventional microstrip Rotman lens is discussed and simulated by HFSS 15 software. A new Rotman lens design including nonuniform distribution of output ports is presented in Section 3, where the fabricated Rotman lens and corresponding measurements are detailed. It is shown that good agreement between measurements and simulation results is achieved.

2. Conventional microstrip Rotman lens

The Rotman lens is a wideband BFN that provides multiple beams covering a wide scanning angle using shaped input and output curves. The geometry of a typical Rotman lens is demonstrated in Figure 1. Exciting any input port results in a wave front with a different phase distribution over the output curve and hence beam steering in the desired direction is achieved. Therefore, the number of input ports determines the steps of scanning. Moreover, the number of output ports specifies the desired directivity of the antenna array. It should be mentioned that the output ports are connected to the antenna array through 50Ω transmission lines with specified lengths.

We assume that the relative electric permittivity of the medium between input and output ports together with the transmission line medium is ϵ_r. The Rotman lens consists of three focal points: G_1, G_2, and G_3. The scan angles (Ψ_α) corresponding to G_1, G_2, and G_3 are 0, ϕ, and $-\phi$, respectively. The phase-errors associated with these focal points are theoretically zero. Hence, the coordinates of the output contour, (X, Y), and transmission line lengths, W, are determined by solving the following equations [20]:

$$(G_1P) + W = (G_1O) + W_0, \tag{1}$$

$$(G_2P)\sqrt{\epsilon_r} + W\sqrt{\epsilon_r} + Y\sin\phi = (G_2O)\sqrt{\epsilon_r} + W_0\sqrt{\epsilon_r}, \tag{2}$$

$$(G_3P)\sqrt{\epsilon_r} + W\sqrt{\epsilon_r} + Y\sin(-\phi) = (G_3O)\sqrt{\epsilon_r} + W_0\sqrt{\epsilon_r}, \tag{3}$$

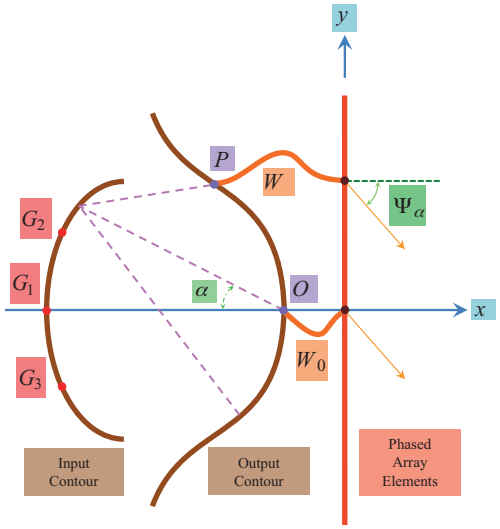

Figure 1. Typical Rotman lens geometry including some important design parameters.

where Y is the y-coordinate of the output ports. The notations (G_iP) and (G_iO) stand for the distance of G_i from P and O, respectively. The transmission line length between O and the central phased array element is W_0. In many applications, more than three input ports are required. The input ports located at nonfocal points are encountered with phase-errors resulting in an undesired array factor (AF). Since the phase-errors can cause beam steering in undesired directions, reducing directivity, and SLL degradation, an optimization algorithm is utilized to design input and output contours. It is assumed that the input ports are located at F_m with $m = \{1 - M\}$ and the output ports are relative to P_n considering $n = \{1 - N\}$. The objective function is defined as follows:

$$OF = \sum_{m=1}^{M} \sum_{n=1}^{N} |L_2 - L_1|, \tag{4}$$

where L_1 is electrical path length from F_m to the central array element. Considering ϕ_m as the desired scan angle associated with F_m, L_2 is electrical path length from F_m to the array element connected to P_n plus demanded phase delay to provide ϕ_m scan angle, as follows:

$$L_2 = (F_mP_n)\sqrt{\epsilon_r} + W_n\sqrt{\epsilon_r} + Y_n \sin\phi_m, \tag{5}$$

$$L_1 = (F_mO)\sqrt{\epsilon_r} + W_0\sqrt{\epsilon_r}. \tag{6}$$

The notations (F_mP_n) and (F_mO) represent the distance of F_m from P_n and O, respectively, whereas W_n and Y_n are the transmission line length and the y-coordinate corresponding to P_n. In this work, a Rotman lens with seven input ports and eight output ports is considered. The design goal of the proposed structure is to provide a scanning angle of -22.5° to 22.5° with 7.5° steps over the X frequency band. In all designed structures, the dielectric substrate is RO4003 with relative electric permittivity of 3.55 and thickness of 32 mil.

The GA optimization algorithm is implemented in MATLAB software, resulting in the designed Rotman lens in Figure 2. According to the symmetry, it is sufficient to detail the (x, y) coordinates of F_1 to F_4, which are (6.10,41.25) mm, (5.23,28.04) mm, (1.32,14.25) mm, and (0,0), respectively. Moreover, (x, y) coordinates of P_1 to P_4 are (161.04,37.44) mm, (164.53,29.23) mm, (166.48,18.78) mm, and (167.54,6.35) mm, respectively.

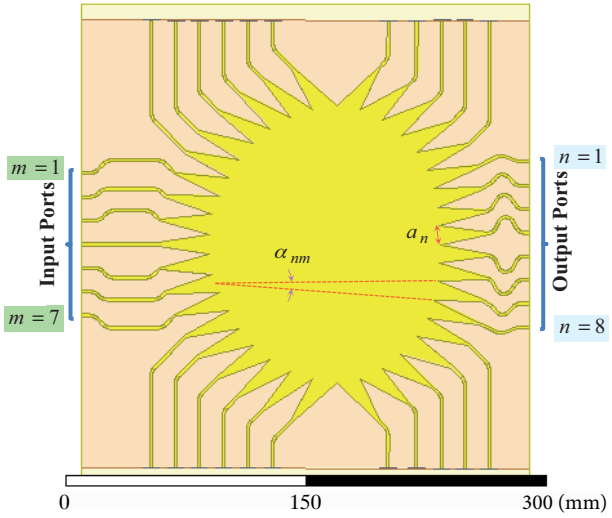

Figure 2. Top view of the designed conventional microstrip Rotman lens with seven input ports and eight output ports.

The initial width of the nth output port is defined by a_n and α_{nm} is the subtended angle through which the nth output port is observed from the mth input port. It is noted that the width of the 50Ω microstrip lines is 2.025 mm. Moreover, the proposed structure occupies $28.32 \times 28.41\text{cm}^2$ and the initial width values of output ports with $n = 1$ to 4 are 12.27 mm, 12.05 mm, 11.86 mm, and 11.78 mm, respectively. The simulated normalized AFs at 8, 10, and 12 GHz, generated by exciting four input ports, are shown in Figures 3a–3c, respectively. The simulated S-parameters are investigated using HFSS software and can be used to obtain the corresponding AF as follows:

$$AF_m = \sum_{n=1}^{8} |S_{n_m}| e^{j[\angle S_{n_m} + k(n-1)d\sin\theta]}, \tag{7}$$

where AF_m is the relative AF of the m^{th} input port obtained using corresponding S-parameters. The spacing between two adjacent elements (output ports) is $d = 16.87$ mm, and the desired scan angles are $\phi_m = 0, \pm 7.5°, \pm 15°, \pm 22.5°$.

The corresponding SLL values for different scan angles at various frequencies are reported in Table 1. It can be seen that SLL varies from 11.73 to 12.44 dB at the central frequency, which is less than the 13 dB upper limit. The simulated scan angles for different input ports at various frequencies are reported in Table 2. It is noted that simulated scan angles are in good accordance with desired ones, showing acceptable errors according to side walls [17]. In order to improve the SLL, the idea of altering parameters a_n and α_{nm} will be considered in the following section.

3. Microstrip Rotman lens with improved SLL

In this section, enhancing the SLL of the Rotman lens is presented without using any additional attenuators or amplifiers. To overcome the previously mentioned 13 dB upper limit for the resulting SLL, a_n parameters (Figure 2) are decreased from the origin ($n = 4, 5$) to the edge of the lens ($n = 1$ or 8). Here, a Chebyshev distribution with corresponding amplitudes in Table 3 is assumed. Due to the symmetry of the Rotman lens, the associated amplitudes with $n = \{1 - 4\}$ are sufficient to be detailed. These amplitudes are applied to the

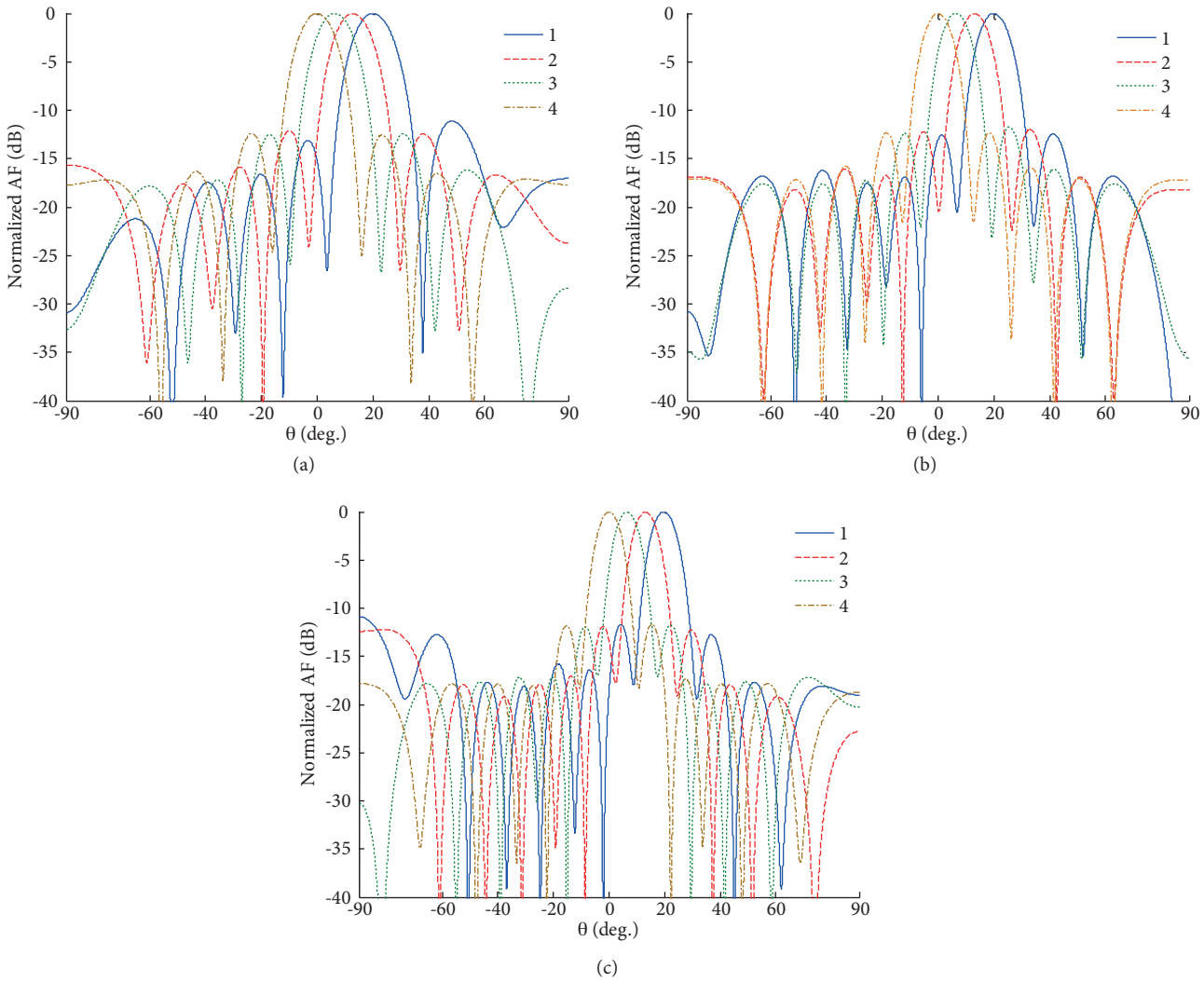

Figure 3. Simulated normalized AFs of the structure specified in Figure 2 using Eq. (7) when the input ports with $m = 1 - 4$ are excited considering a) $f = 8$ GHz, b) $f = 10$ GHz, and c) $f = 12$ GHz.

distribution of a_n, resulting in a structure with different initial width of the output ports, which is shown in Figure 4.

Now attempts are made to introduce a theoretical background for the resultant AF of the proposed Rotman lens. It is more accurate to consider α_{nm} instead of a_n in the procedure of defining the excitation amplitudes of the output array. Therefore, the corresponding values of α_{nm} are calculated and normalized to the respective maximum value (Table 4). It is obvious that the excitation of the corner input port (1/1–1/8 corresponding values in Table 4) is the case least suited to the Chebyshev distribution in Table 3. Therefore, it is expected not to achieve a remarkable SLL improvement when this input port is excited.

The proposed theory is based on assumptions that the wave front reaches the output ports without any phase-error together with the amplitude distribution defined by α_{nm}, i.e.

$$AF_m^{\text{theory}} = \sum_{n=1}^{8} \alpha_{n_m} e^{jk(n-1)d(\sin\theta - \sin\phi_m)}, \tag{8}$$

Table 1. SLLs (dB) of AFs in Figures 3a–3c for different input ports at various frequencies.

Frequency (GHz)	Input port	SLL (dB)
8	1	11.10
8	2	12.09
8	3	12.46
8	4	12.41
10	1	12.44
10	2	11.97
10	3	11.73
10	4	12.32
12	1	11.68
12	2	11.89
12	3	11.72
12	4	11.64

Table 2. Scan angles of AFs in Figures 3a–3c for different input ports at various frequencies.

Frequency (GHz)	Input port	Scan angles
8	1(22.5°)	20.01°
8	2(15°)	12.83°
8	3(7.5°)	6.37°
8	4(0)	0
10	1(22.5°)	19.98°
10	2(15°)	13.08°
10	3(7.5°)	6.44°
10	4(0)	0
12	1(22.5°)	19.7°
12	2(15°)	13.19°
12	3(7.5°)	6.53°
12	4(0)	0

Table 3. Utilized Chebyshev distribution.

Output port	Amp.
1	0.58
2	0.66
3	0.87
4	1

where AF_m^{theory} is the theoretical AF when the mth input port is excited considering theoretically isotropic radiating antennas at output ports. The theoretically calculated normalized AFs at 8, 10, and 12 GHz are shown in Figures 5a, 5b, and 5c, respectively. The obtained SLLs considering different input ports are about 17.7 dB at various frequencies.

Now the designed Rotman lens with altered initial width of output ports is simulated using HFSS 15, fabricated, and tested. The schematic view of the fabricated proposed Rotman lens and measurement setup is illustrated in Figures 6a and 6b, respectively. The width values of output ports with $n = 1$ to 4 are 8.94 mm,

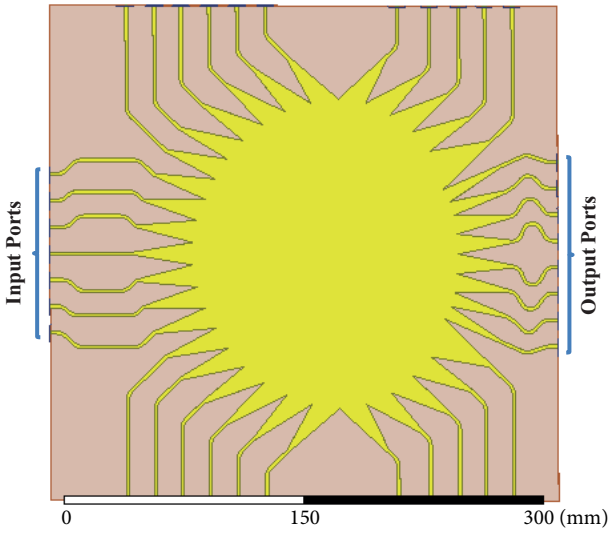

Figure 4. Top view of designed microstrip Rotman lens with altered initial width of output ports according to the Chebyshev distribution in Table 3.

Table 4. Normalized α_{nm}.

Input/output port	Normalized distribution	Input/output port	Normalized distribution
1/1	0.66	3/1	0.67
1/2	0.73	3/2	0.72
1/3	0.98	3/3	0.97
1/4	1.00	3/4	1.00
1/5	0.99	3/5	1.00
1/6	0.93	3/6	0.95
1/7	0.69	3/7	0.71
1/8	0.69	3/8	0.68
2/1	0.67	4/1	0.68
2/2	0.72	4/2	0.71
2/3	0.98	4/3	0.96
2/4	1.00	4/4	1.00
2/5	0.99	4/5	1.00
2/6	0.94	4/6	0.96
2/7	0.70	4/7	0.71
2/8	0.69	4/8	0.68

9.07 mm, 12.24 mm, and 12.72 mm, respectively. The reflection coefficients of the Rotman lens considering the input ports with $m = \{1 - 4\}$ and the output ports determined by $n = \{1 - 4\}$ are measured in the X-band (Figures 7a and 7b). According to the symmetry of the designed structure, Figures 7a and 7b show good matching at all input and output ports. Therefore, in view of the reflection coefficient, the proposed method of altering the a_n parameters does not disturb the performance of the Rotman lens. The measured S-parameters can be used to obtain the corresponding AF utilizing Eq. (7). It is noted that the Rotman lens insertion loss is inherently considered in radiation pattern calculations due to utilization of measured S-parameters.

The simulated and measured normalized AF patterns for different input ports ($m = 1, 2, 3, 4$) at 10 GHz are demonstrated in Figures 8a, 8b, 8c, and 8d, respectively. It is mentionable that AF patterns are calculated

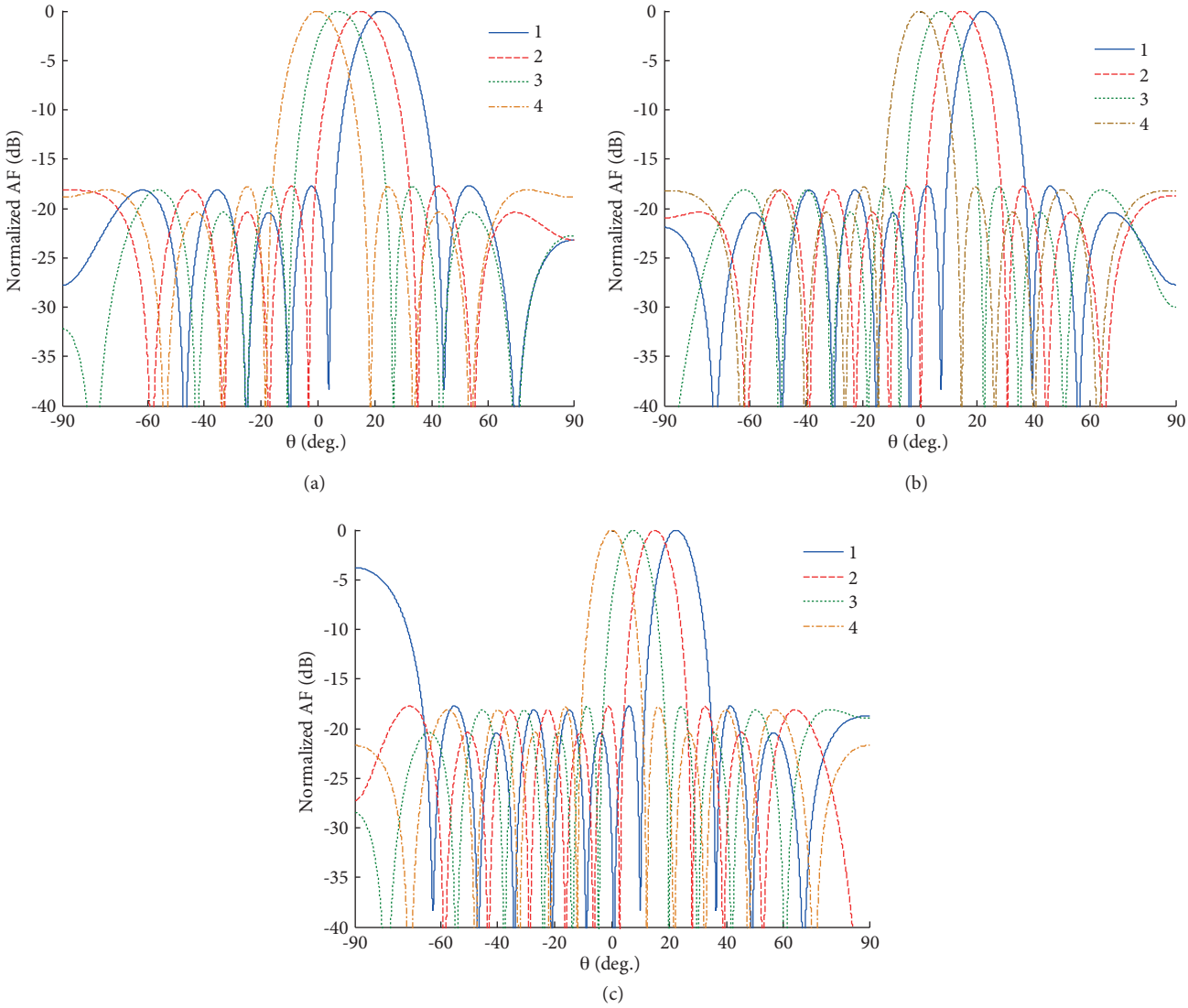

Figure 5. Theoretically calculated normalized AFs using Eq. (8) and the values in Table 4, considering the input ports with $m = 1 - 4$ and a) $f = 8$ GHz, b) $f = 10$ GHz, and c) $f = 12$ GHz.

utilizing corresponding S-parameters considering isotropic radiating elements connected to output ports in Eq. (7). According to the symmetry of the designed Rotman lens, $m = 1$–4 are sufficient to be studied. Since X-band application is of interest, the performance of the proposed lens is further investigated in frequencies of 8 GHz and 12 GHz as the middle input port is excited (Figures 9a and 9b). Good agreement between simulated and measured results can be observed, whereas a little SLL degradation is due to some imperfections in the measurement procedure such as from SMA connectors, matched loads, and surrounding absorbers. Some of these unwanted error sources most affect the results associated with the corner input ports.

For more investigations, Table 5 compares the relative simulated and measured SLLs considering different input ports and various frequencies. In the case where the excitation port is off-center, the preassumptions under which Eq. (8) is proposed are not well met, e.g., the assumption that no phase-error at the array elements can be highly deteriorated due to reflections from the side walls. The comparison between results in Tables 1 and 5

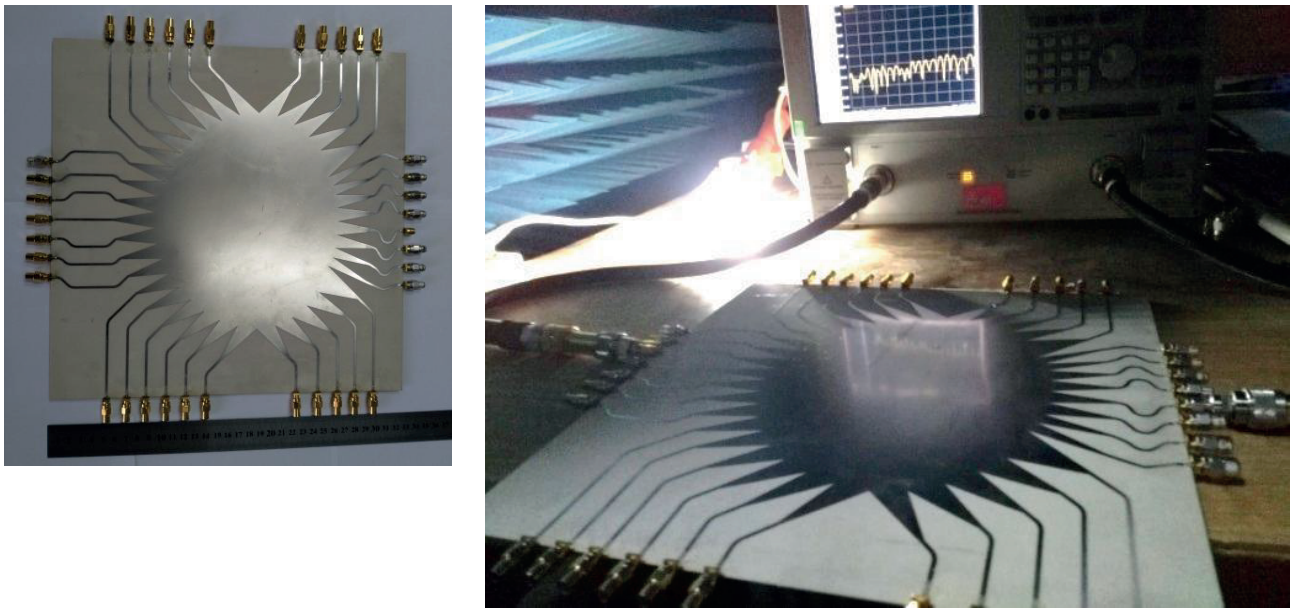

(a) (b)

Figure 6. a) Fabricated Rotman lens; b) measurement setup.

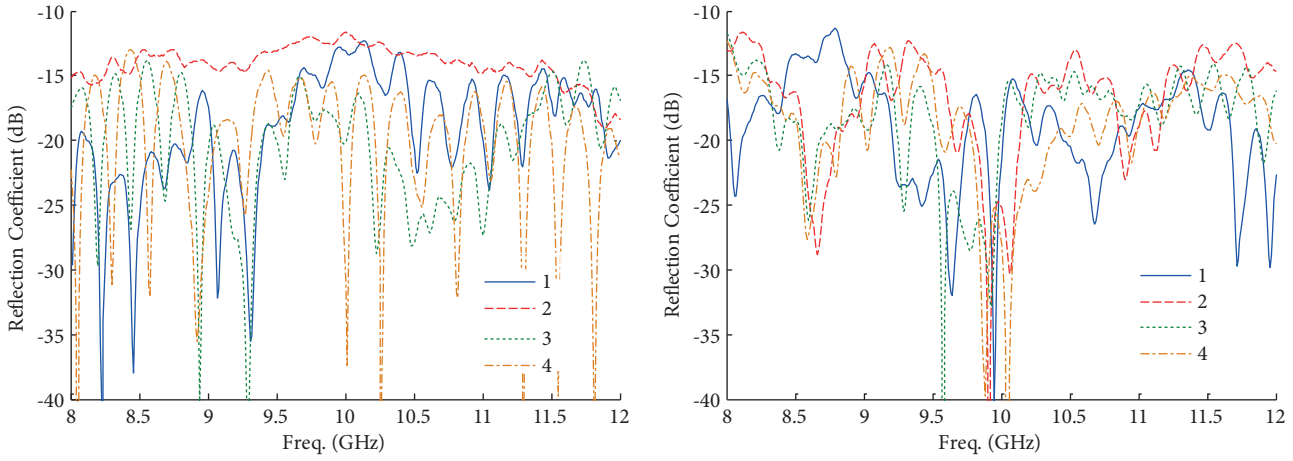

Figure 7. Measured results for reflection coefficients of the structure shown in Figure 6a considering X-band operation frequencies and the excitation of a) input ports with $m = 1 - 4$ and b) output ports with $n = 1 - 4$.

at the central operating frequency shows 3.13 and 4.61 dB SLL improvement when the input ports with $m = 4$ and 3 are excited, respectively. As expected, the main drawback is addressed when the corner input port is excited. It is concluded that the SLL has been improved when the input ports with $m = 4$ and 3 are excited at all 8, 10, and 12 GHz operating frequencies.

Now the presented Rotman lens is investigated in view of resultant scan angles. The simulated and measured scan angles of the structure shown in Figure 6a for different input ports and various frequencies are reported in Table 6. The comparison between results in Tables 2 and 6 justifies that the scan angles of the proposed Rotman lens (Figure 4) more accurately follow the desired scan angles than those of the conventional

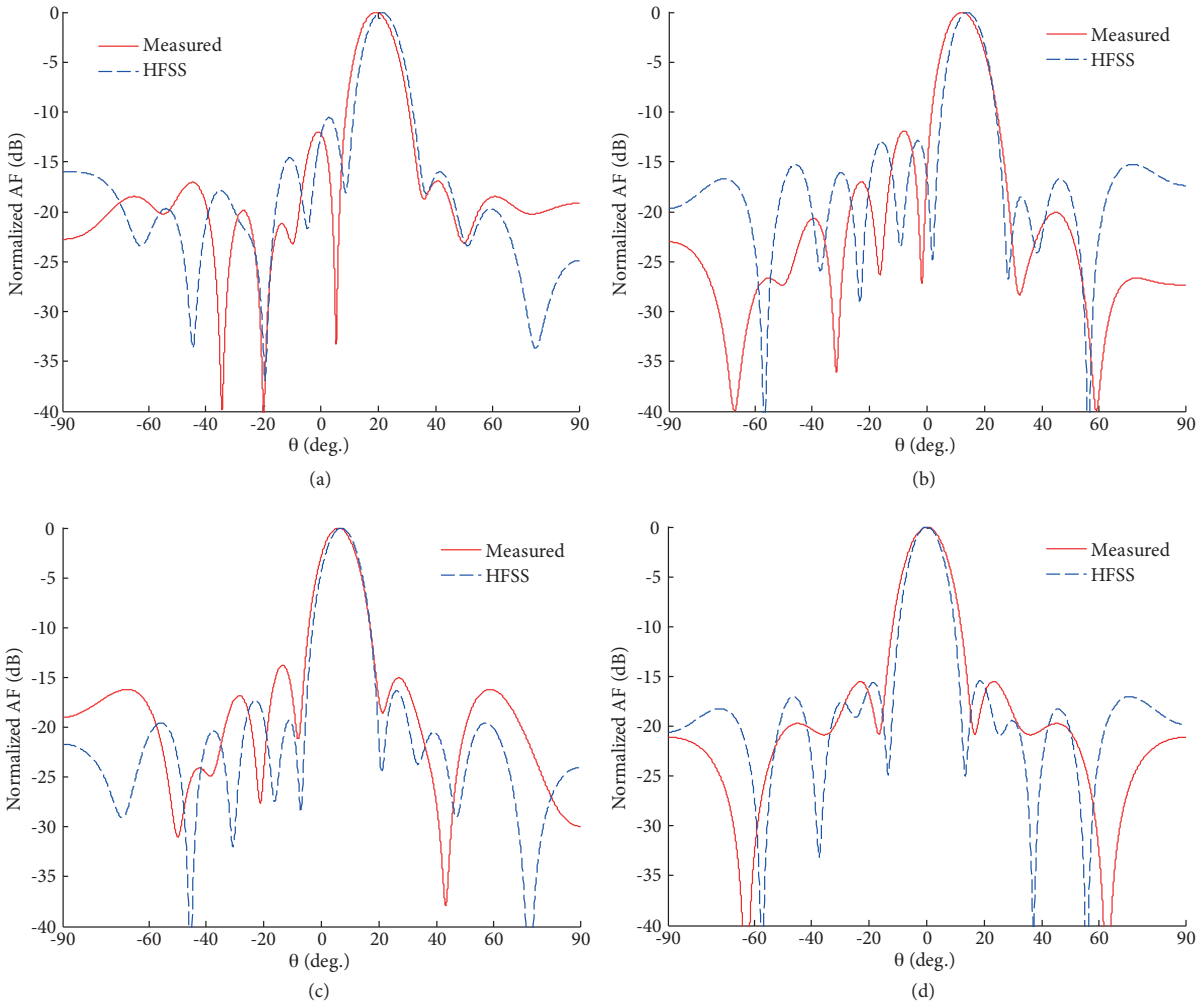

Figure 8. Normalized AFs of the structure shown in Figure 6a at 10 GHz using simulated and measured S-parameters together with Eq. (7), corresponding to the input ports with m = a) 1, b) 2, c) 3, and d) 4.

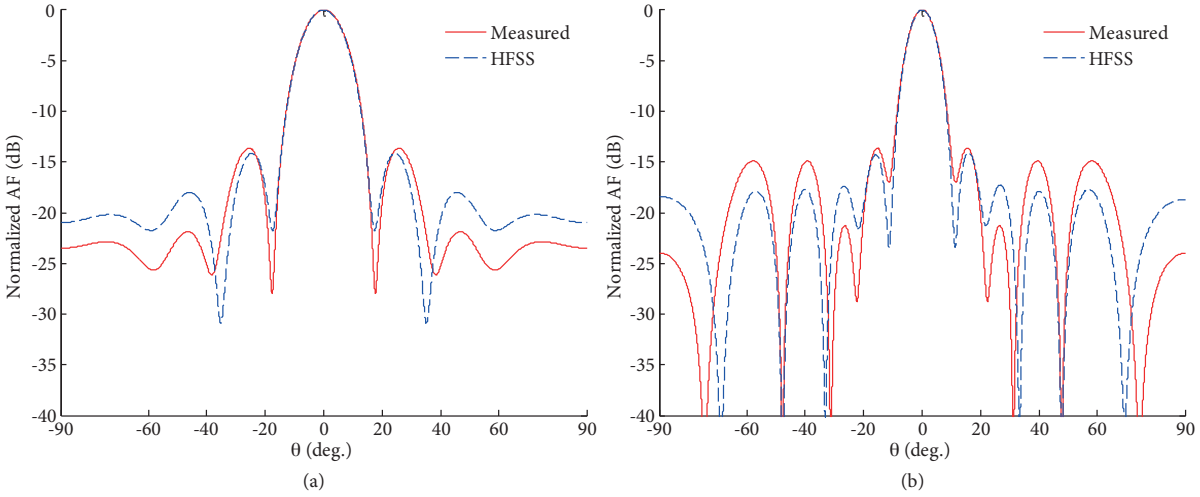

Figure 9. Normalized AFs of the structure shown in Figure 6a using simulated and measured S-parameters together with Eq. (7), when the middle input port is excited at a) f = 8 GHz and b) f = 12 GHz.

Table 5. SLLs (dB) of AFs associated with the structure shown in Figure 6a for different input ports at various frequencies.

Frequency (GHz)	Input port	SLL simulation	SLL measurement
8	1	11.35	9.46
8	2	12.16	13.20
8	3	13.20	12.71
8	4	14.14	13.64
10	1	10.54	11.99
10	2	12.85	11.90
10	3	16.34	13.76
10	4	15.45	15.52
12	1	10.43	11.73
12	2	10.84	12.68
12	3	12.76	12.98
12	4	14.06	13.64

Table 6. Scan angles of AFs associated with the structure shown in Figure 6a for different input ports at various frequencies.

Frequency (GHz)	Input Port	Scan Angle (Theory) (°)	Scan Angle (Sim.) (°)	Scan Angle (Meas.) (°)
8	1	22.5	18.93	19.77
8	2	15	12.59	12.28
8	3	7.5	6.26	6.26
8	4	0	0	0
10	1	22.5	21.20	19.05
10	2	15	14.10	12.06
10	3	7.5	6.90	5.90
10	4	0	0	0
12	1	22.5	19.06	19.66
12	2	15	12.58	12.69
12	3	7.5	6.21	6.59
12	4	0	0	0

Rotman lens (Figure 2). According to the applied Chebyshev distribution in Table 3, corner output ports are narrower in comparison to those of the conventional structure. Moreover, these output ports are more affected by side wall reflections than middle ones. Based on the reduced width of corner output ports, resulting errors are decreased in the proposed structure. Therefore, more accurate scan angles are achieved.

4. Conclusion

In this paper, a new X-band microstrip Rotman lens with improved SLL has been proposed. A proper distribution of output ports with different initial width values is considered to improve the resultant SLL. The benefit of SLL improvement is not based on using additional attenuators or amplifiers at the output ports. A new AF analysis is introduced for the proposed Rotman lens, producing a good estimation of SLL improvement. Simulation results show more than 3 dB of SLL enhancement in the case of excitation of the middle input port at the central operating frequency. The advantage of SLL improvement is observed at all

noncorner scan angles at 10 GHz. Moreover, the proposed Rotman lens yields more accurate scan angles than the conventional structure. The proposed Rotman lens has been fabricated and measured. Good agreement between the simulated and measured results has been achieved.

References

[1] Rodenbeck CT, Kim SG, Tu WH, Coutant MR, Hong S, Li M, Chang K. Ultra-wideband low-cost phased-array radars. IEEE T Microw Theory Tech 2005; 53: 3697–3703.

[2] Metz C, Grubert J, Heyen J, Jacob AF, Janot S, Lissel E, Oberschmidt G, Stange LC. Fully integrated automotive radar sensor with versatile resolution. IEEE T Microw Theory Tech 2001; 49: 2560–2566.

[3] Parker D, Zimmermann DC. Phased arrays–part II: implementations, applications and future trends. IEEE T Microw Theory Tech 2002; 50: 2097–2103.

[4] Vashist S, Soni MK, Singhal PK. A review on the development of Rotman lens antenna. Chinese Journal of Engineering 2014; 2014: 385385.

[5] Ruze J. Wide-angle metal-plate optics. P IRE 1950; 38: 53-58.

[6] Gent H. The bootlace aerial. Royal Radar Establishment Journal 1957; 10: 47-57.

[7] Rotman W, Turner RF. Wide-angle microwave lens for line source applications. IEEE T Antenn Propag 1963; 11: 623–632.

[8] Shelton JP. Focusing characteristics of symmetrically configured bootlace lenses. IEEE T Antenn Propag 1978; 26: 513–518.

[9] Katagi T, Mano S, Sato S. An improved design method of Rotman lens antennas. IEEE T Antenn Propag 1984; 32: 524–527.

[10] Hansen RC. Design trades for Rotman lenses. IEEE T Antenn Propag 1991; 39: 464–472.

[11] Rao J. Multifocal three-dimensional bootlace lenses. IEEE T Antenn Propag 1982; 30: 1050–1056.

[12] Rao J. Correction to Multifocal three-dimensional bootlace lenses. IEEE T Antenn Propag 1983; 31: 541.

[13] Schulwitz L, Mortazawi A. A new low loss Rotman lens design using a graded dielectric substrate. IEEE T Microw Theory Tech 2008; 56: 2734–2741.

[14] Maybell MJ. Printed Rotman lens fed array having wide bandwidth, low side lobes, constant beamwidth and synthesized radiation pattern. IEEE AP-S 1983; 21: 373–376.

[15] Kilic O, Dahlstrom R. Rotman lens beam formers for army multifunction RF antenna applications. In: Proceedings of IEEE Antennas and Propagation Society International Symposium; 2005. pp. 43–46.

[16] Stutzman WL, Thiele GA. Antenna Theory and Design. New York, NY, USA: Wiley, 1998.

[17] Darvazehban A, Manoochehri O, Salari MA, Dehkhoda P, Tavakoli A. Ultra-wideband scanning antenna array with Rotman lens. IEEE T Microw Theory Tech 2017; 65: 3435–3442.

[18] Li WR, Chu CY, Lin KH, Chang SF. Switched-beam antenna based on modified Butler matrix with low sidelobe level. Electron Lett 2004; 40: 290–292.

[19] Rausch EO, Peterson AF. Rotman lens design issues. In: Proceedings of IEEE Antennas and Propagation Society International Symposium and USNC/URSI Meeting; 2005. pp. 35–38.

[20] Dong J, Zaghloul AI, Rotman R. Phase-error performance of multi-focal and non-focal two-dimensional Rotman lens designs. IET Microw Antennas Propag 2010; 4: 2097–2103.